chemosensors

MDPI

Article

"Coffee Ring" Fabrication and Its Application in Aflatoxin Detection Based on SERS

Xuesong Yan [1,2,†], Wenfeng Zhu [1,3,†], Yibing Wang [4,†], Yiran Wang [1], Dexuan Kong [1] and Min Li [1,*]

[1] CAS Key Laboratory for Biomedical Effects of Nanomaterials and Nanosafety, Institute of High Energy Physics, The Chinese Academy of Sciences, Beijing 100049, China
[2] College of Matericals Science & Engineering, Heibei University of Science and Technology, Shijiazhuang 050018, China
[3] Department of Biochemistry and Molecular Biology, Institute of Basic Medical Sciences, Chinese Academy of Medical Sciences and Peking Union Medical College, Beijing 100005, China
[4] School of Biotechnology, East China University of Science and Technology, Shanghai 200237, China
* Correspondence: limin@ihep.ac.cn
† These authors contributed equally to this work.

Abstract: The fabrication of a coffee ring was studied in this work to improve its sensitivity in detecting trace analytes based on surface-enhanced Raman scattering (SERS). Gold nanoparticles were synthesized with diameters of ~40 nm through the sodium citrate reduction method, and rhodamine 6G (R6G) was employed as a probe to evaluate the performance of the fabricated coffee rings. The results showed that the coffee ring formed from the water-washed gold nanoparticles presented more orderly and regular morphology as well as better SERS properties than the unwashed ones. Furthermore, both the concentration and the amount of gold nanoparticles were found to affect its SERS performance. Using the optimized coffee ring as a SERS substrate, trace R6G with a concentration of 5×10^{-8} M was detected. This sensing platform could realize aflatoxin B1 (AFB1) detection down to 5×10^{-7} M and was demonstrated to function well in real-sample testing.

Keywords: coffee ring effect; surface-enhanced Raman scattering (SERS); aflatoxin B1 detection

Citation: Yan, X.; Zhu, W.; Wang, Y.; Wang, Y.; Kong, D.; Li, M. "Coffee Ring" Fabrication and Its Application in Aflatoxin Detection Based on SERS. *Chemosensors* **2023**, *11*, 22. https://doi.org/10.3390/chemosensors11010022

Academic Editor: Barbara Palys

Received: 24 November 2022
Revised: 21 December 2022
Accepted: 21 December 2022
Published: 26 December 2022

1. Introduction

Surface-enhanced Raman spectroscopy (SERS) has become a powerful sensing technique due to its high sensitivity, nondestructive features and rapid detection [1–3]. It has been widely used in many fields including biomedicine, environmental science, food safety and others [4–8]. SERS mainly derives from the local surface plasmon resonance (LSPR) characteristics of precious metal nanoparticles, which can significantly enhance Raman signals by several orders of magnitude [9,10]. Gold and silver nanoparticles are the most widely used noble metal SERS substrate materials, and they can present a strong enhancement effect from "SERS active-nanogaps" through aggregation. "Coffee ring" refers to a phenomenon that when a drop of coffee dries on a solid surface, its suspended particulate matter deposits along the original perimeter, leaving a ring-like stain. This phenomenon was first investigated by Deegan et al. [11] and was observed with many colloidal suspensions. The "coffee ring" effect refers to the evaporation of a dried colloidal sessile drop, including gold or silver nanoparticles (it can be other nanoparticles), on a solid surface, forming a dense ring array at the boundary where many "hot spots" are fabricated through the aggregation of the metal nanoparticles [11,12]. In the process of coffee ring formation, the three-phase contact angle between the atmosphere, the droplet and the solid substrate is fixed. Due to the evaporation of the solvent, the nanoparticles are forced to flow from the inside of the droplet to outside, resulting in significant capillary flow. However, the optimization of various conditions to obtain better effects of the coffee ring on SERS enhancement has been less widely investigated.

The "coffee ring" effect has received considerable attention thanks to its important applications in the field of sensing. Xu and coworkers [13] introduced the gold coffee ring effect to detect six kinds of polycyclic aromatic hydrocarbons with a limit of detection (LOD) of 10^{-6} M via SERS. Wang [14] et al. realized the sensitive detection of malachite green and arsenate to 0.1 ng/L and 0.03 mg/L, respectively, based on the silver coffee effect. Wu [15] and coworkers used SA-AgNPs as the SERS substrate and further employed the coffee ring effect to detect the illegal adulteration of the chemicals Gordenafil and Rosiglitazone maleate in health care products to ug/mL. Gao [16] developed a blood serum analysis approach to screen different types of cancers through coffee-ring-effect-assisted SERS technology. Pan [17] et al. prepared a β-CD-coated Ag NP (AgNP@β-CD) to form a coffee ring for the SERS detection of aromatic compounds OPD with an LOD of 10^{-10} M. Though the "coffee ring" effect has been used in many applications for trace target detection, no one has reported its use in aflatoxin detection.

Mycotoxins are toxic and carcinogenic secondary metabolites produced by various molds. They cause serious harm to human health by contaminating various foods and animal feeds [18,19]. In recent years, aflatoxins (AFBs) have often been found in agricultural products. A series of economic losses, as well as the potential risks to food and feed, mean that mycotoxins pollution has attracted global attention [20]. Among several types of aflatoxins, aflatoxin B1 (AFB1) is most toxic and has been classified as a Class I carcinogen by the International Agency for Research on Cancer (IARC) [21]. AFB1 is especially harmful to the human liver. The clinical manifestations of a small amount of AFB1 exposure include loss of appetite, nausea and vomiting. Exposure to a large amount of AFB1 can cause liver cirrhosis, necrosis and cancer. In the past few decades, a lot of research has been carried out on the development of analytical methods for the qualitative/quantitative detection of chemical contaminants in food, including aflatoxins. The main detection methods of AFB1 are usually electrochemistry (EC), high-performance liquid chromatography (HPLC), liquid chromatography combined with mass spectrometry (LC-MS), enzyme-linked immunosorbent assay (ELISA), cyclic voltammetry (CV), aptasensors, etc., with the detection limits of microgram per kilogram (μg/kg), nano to pico-molar, or even at the ppb level [22–27]. These methods are effective in AFB1 detection but with limitations, such as cumbersome sample processing, toxic treatment reagents, expensive equipment, complicated operations and lengthy analysis times [28,29]. Therefore, the development of approaches for AFB1 detection with high sensitivity and simplicity is highly desirable.

This work reported the optimization of conditions for the fabrication of coffee rings with high sensitivity and reproducibility. Using an as-prepared coffee ring as the SERS substrate, the detection limit for R6G was 5×10^{-8} M. This sensing platform could realize AFB1 detection down to 5×10^{-7} M, further suggesting its sensitivity for the determination of trace analytes of interest.

2. Materials and Methods

2.1. Materials

Tetrachloroauric acid trihydrate, Alfa Aesar (China) Chemical Co., Ltd.; Trisodium Citrate, 99.0%, Alfa Aesar (Shanghai, China) Chemical Co., Ltd.; Aflatoxin (AFB1), Beijing Yinuokai Technology Co., Ltd. (Beijing, China); Rhodamine 6G (R6G, Aladdin Reagent Company (Shanghai, China)).

2.2. Instruments and Measurements

Scanning electron microscopy (SEM) characterization was undertaken using a Hitachi S-4800 at 30 kV. A UV-3600 plus ultraviolet-visible spectrophotometer, Shimadzu Corporation, Japan, was used. The DXR Smart Raman spectrometer (Thermo Fisher Scientific, Waltham, MS, USA) had an excitation wavelength of 780 nm, maximum excitation power of 80 mw and integration time of 15 s. The laser Raman spectrometer (Renishaw, UK) had an excitation wavelength of 785 nm, maximum excitation of power 1 mw, 5 mw and 10 mw and integration time of 10 s, equipped with a microscope Raman detection platform (50× objective lens).

2.3. Preparation of Gold Nanoparticles

The gold nanoparticles were synthesized using a reported method [30]. In brief, 150 mL of 2.2 mmol/L sodium citrate solution was added into a 250 mL three-necked flask which was put into an oil bath pan. The solution was heated to 100 °C and boiled vigorously with stirring for 15 min. Then, 1 mL of $HAuCl_4$ (25 mmol/L) was added, and the color changed from yellow to blue gray and finally to pink within 10 min. The reaction was cooled down to 90 °C before adding 1 mL of sodium citrate (60 mmol/L). Then, 2 min later, 1 mL of $HAuCl_4$ (25 mmol/L) was added, and 30 min later, the 2 mL solution was taken out as the first generation of nanoparticles. This process was repeated until the 14th generation of nanoparticles was obtained, which were used in this work.

2.4. Wafer Hydrophobic Treatment

The silicon wafers were first ultrasonically cleaned in ethanol and acetone for 10 min and thoroughly cleaned with piranha solution at 95 °C for 40 min (H_2SO_4:H_2O_2 = 3:1, *v*/*v*; the solution should be handled with great care). After being rinsed with the triple-distilled water and dried under gaseous N_2 flow, the cleaned silicon wafers were immersed in a 10% hydrogen fluoride solution for 10 min to remove the oxide layer on the wafer. The silicon wafers were then rinsed with triple-distilled water, dried with gaseous N_2 flow and kept for further use.

The surface property of the silicon wafer was tested and compared by dropping a droplet of Au NP colloid onto the surface after and without hydrophobic treatment.

2.5. Preparation of Coffee Ring

The synthesized gold nanoparticles were washed with triple-distilled water before being centrifuged at 7000 rpm/min twice. Then, the gold nanoparticles were concentrated by 2×, 4×, 6×, 8×, 10×, 20×, 40×, 60× and 80×(different concentration times) and mixed with R6G solution in a ratio of 1:1, respectively. The 4 × concentrated Au NP colloid was selected and mixed with R6G solution. Then, the 1 µL, 2 µL, 3 µL, 4 µL and 5 µL mixtures were dropped onto the silicon wafer to form the coffee ring for SERS detection. Since AFB1 is hard to dissolve in water, AFB1 was firstly dissolved in acetonitrile at a high concentration and then diluted with triple-distilled water for the preparation of different-concentration solutions. Then, the AFB1 solution with a special concentration was mixed with 4 times the concentrated gold nanoparticle colloid before dropping the 1 µL mixture onto the silicon wafer to form the coffee ring for SERS detection. It took around 20 min for the coffee ring to dry on silicon. SERS spectra were recorded and collected on a DXR Smart Raman spectrometer (Thermo Fisher Scientific, Waltham, MS, USA; 780 nm; 80 mW; 10 µm diameter focal spot laser excitation; 15 s integration time; room temperature).

2.6. Preparation of Food Samples

Corn, peanut flour and sesame samples were crushed into powder and dispersed in water (20 mg/g) followed by centrifuging. AFB1 was firstly dissolved in acetonitrile with a high concentration before it was further diluted with triple-distilled water for the preparation of AFB1 solutions with different concentrations. AFB1 solutions with concentrations of 3×10^{-5} M and 3×10^{-6} M for corn, 2×10^{-5} M and 4×10^{-6} M for peanut and 4×10^{-5} M for sesame were added into the sample supernatant followed by sonication. Then, 10 µL of this sample solution was added into 20 µL of the 4-times-concentration Au NP colloid before mixing them thoroughly. The 1 µL mixture was dropped onto the silicon wafer to form the coffee ring for SERS detection.

3. Results and Discussion

The morphology of the gold nanoparticles characterized via scanning electron microscope (SEM) and the UV-3600 ultraviolet spectrometer is shown in Figure 1a,b. The synthesized gold nanoparticles were uniform in size and were mostly distributed at around 40 nm in diameter, which agreed well with the previously reported work [30]. The concentration

of gold nanoparticles was approximately ~3 × 10^{12} NPs/mL according to the literature [30]. It is noteworthy that the shape of the gold nanoparticles was not theoretically spherical, but with different crystal planes, as seen in the SEM image (Figure 1a). These crystal planes closely faced each other and were arranged in parallel or vertical, as indicated by the circles in Figure 1a, which could largely increase the number of "hot spots" and consequently contribute more to the Raman signal enhancement. As expected, the corresponding extinction spectra of gold nanoparticles resulted in a UV absorption peak at 524 nm, as presented in Figure 1b, which presents an intrinsic UV peak location of gold. Figure 1c schematically shows the process of optimizing the coffee ring effect and detecting the analyte of interest. Noticeably, washing, concentrating and controlling the volume of gold colloids are the key points in fabricating a coffee ring as an excellent SERS substrate.

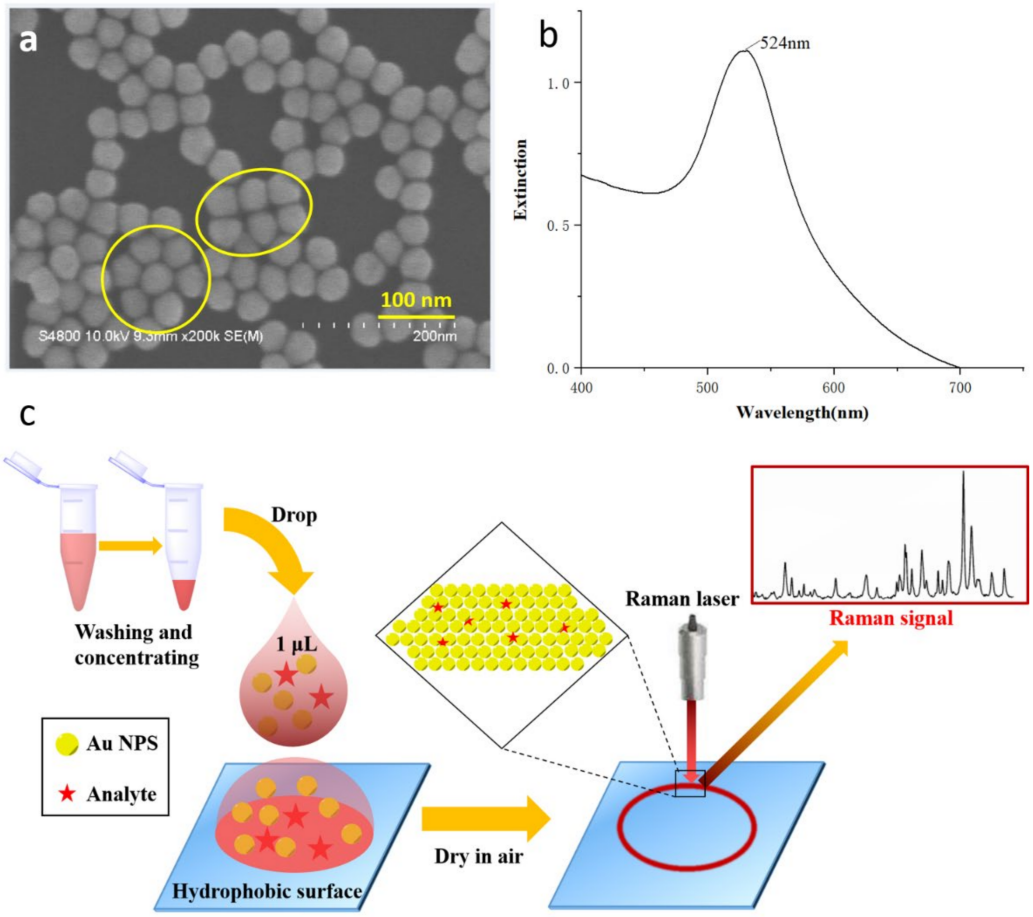

Figure 1. (**a**) SEM and (**b**) UV−vis spectrum of the as-prepared Au NPs. (**c**) Schematic process cartoon of the optimization of coffee ring effect and analyte detection.

Figure 2 shows the edge morphology of the coffee rings formed from both unwashed and washed gold nanoparticles, which were characterized by SEM and a Raman spectrometer (maximum excitation power of 5 mw), respectively. It could be clearly seen that the Au NPs in the as-synthesized gold colloid without washing were unevenly distributed on the edge of the coffee ring (Figure 2a). This phenomenon was possibly caused by the presence of citrate sodium in solution. Citrate sodium is normally used as a stabilizer for gold nanoparticles in solution since the negatively charged carboxylic acid ions extend outwards and could create electrostatic repulsion, which prevents gold nanoparticles from aggregating effectively. The edge of the coffee ring formed from the washed Au NPs looked neater and more regular compared with the unwashed one, as presented in Figure 2b. This indicates the gold nanoparticles could aggregate easily after removing the citrate sodium. A photograph is provided in the inset of Figure 2b, showing the wettability of

the silicon surface before and after hydrophobic treating with hydrofluoric acid. After one droplet of the washed gold colloid was deposited on the silicon surface, the untreated one (right) made water spread at the periphery of the silicon surface, while the treated one (left) enabled the droplet shape to be maintained to a certain extent, indicating the surface after treatment (right) was hydrophobic. To compare the performance of the coffee rings from washed and unwashed gold colloid, a typical dye molecule, rhodamine 6G (R6G), which is considered a classic Raman reporter (with high cross-section), was introduced to be a probe in this system. The Raman curve of the R6G powder was collected and is shown in Figure 2c. The Raman vibration of the 612 cm^{-1} peak corresponds to the bending of the C-C-C ring plane, while 774 cm^{-1} corresponds to the out-of-plane bending vibration of C-H and 1181 cm^{-1} to the bending vibration of both C-H and N-H chemical bonds. The peak at 1305 cm^{-1} is attributed to the stretching vibration of C = C. Additionally, 1364 cm^{-1}, 1509 cm^{-1} and 1649 cm^{-1} correspond to the C-C vibration. Noteworthy is that the Raman signals of R6G in the coffee ring formed from the washed Au NPs are pronouncedly higher than those from the unwashed one, as shown in Figure 2c. In particular, the peak shape of R6G is sharper in the coffee ring formed from the washed gold nanoparticles. This indicates that besides the neat and even ring morphology, the performance of the coffee ring formed from the washed Au NPs is better than that of the unwashed ones. This can be explained from the way citrate sodium stabilizes gold nanoparticles. As is known, two adjacent carboxylic acid roots of citrate sodium adsorb on the surface of gold nanoparticles through coordination, and the other carboxylic acid ions extend outwards, so that the surface of each gold nanoparticle is negatively charged. Owing to that, the gold nanoparticles can stably disperse in aqueous solution through electrostatic repulsion. Therefore, a large amount of citrate sodium in the gold colloid could possibly hinder the effectively aggregation of gold nanoparticles; here, this resulted in the unregular pattern of the ring edge (Figure 2a) and the reduced coffee ring effect on SERS enhancement.

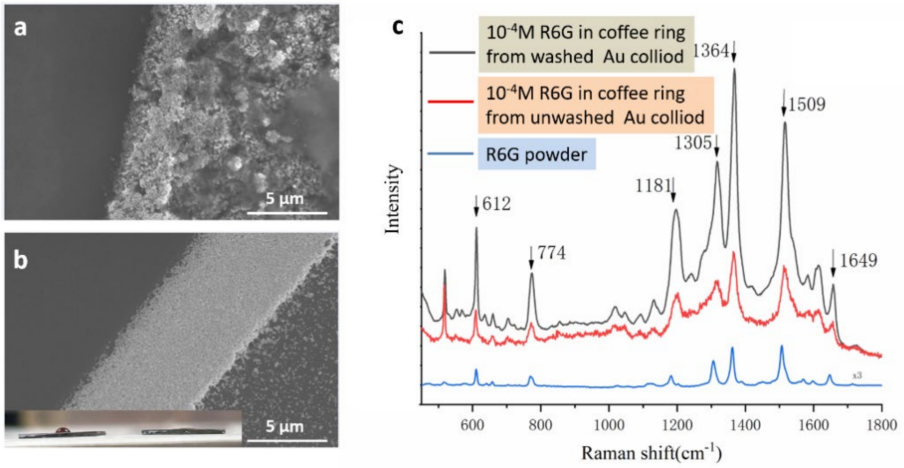

Figure 2. SEM images of the coffee ring edges (**a**,**b**) and the Raman spectra of 10-4M R6G with the coffee ring (**c**) formed from both unwashed and washed Au NPs.

The previous studies show that the distribution density of Au NPs is an important factor to the coffee ring effect [31,32]. According to the mechanism of coffee ring formation, the edge of the gold colloid droplet will be pinned to the solid surface, and the liquid evaporating from the droplet edge will be replenished by the liquid from the interior, which causes a capillary flow that carries dispersed particles to the drop periphery through the evaporation process. When the concentration of Au NPs becomes low, there are not enough gold nanoparticles in the droplet, so the uneven edge morphology of the ring will lead to a lower number of hot spots and thus weaken the Raman intensity of the targets. On the contrary, when the concentration is too high, the effective hot spots at the edge will reduce and thus weaken the Raman signal due to the stacking and aggregation of Au NPs in the

vertical direction. Therefore, the performance of coffee rings prepared from Au NP colloids with different concentrations was investigated in this work.

Figure 3 shows the SEM images of the coffee rings formed from water-washed Au NP colloids with 1×, 10×, 20×, 40×, 60× and 80× concentration times. The morphologies of the whole coffee rings and their local high-resolution images are shown in Figure 3a–f1. The diameter of the coffee rings formed from different concentrated times of Au NPs colloid kept identical and was determined to be around 3 mm.

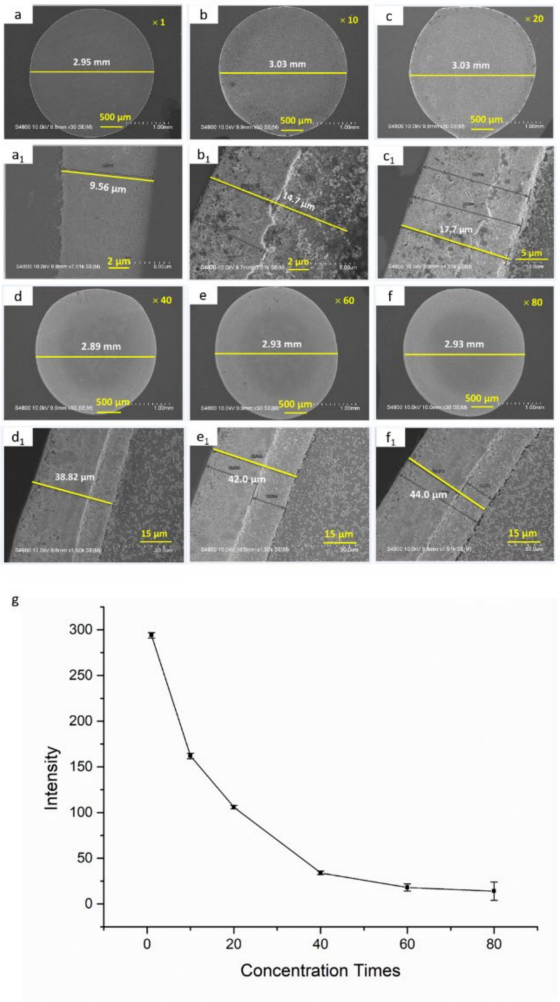

Figure 3. (**a**–**f**$_1$) SEM images of the coffee ring formed from water-washed Au NP colloids with different concentration times. (**g**) The tendency of Raman intensity of 10^{-6} M R6G in the coffee ring with different concentration times of water-washed Au NP colloids based on the peak of 1364 cm^{-1}. The Raman data were collected from the DXR Smart Raman spectrometer (Thermo Fisher Scientific, Waltham, MS, USA): excitation wavelength, 780 nm; maximum excitation power, 80 mw; integration time, 15 s.

The Au NP colloids kept identical and were determined to be around 3 mm. Meanwhile, the edge width of the ring presented a clear upward tendency with increased concentration times, from 9.56 to 44.0 μm, as indicated in Figure 3a1–f1. Interestingly, the Au NPs at the edges were observed to start distributing unevenly, and a particle line appeared at the edge when the concentration times was higher than 10. The white line could have resulted from the formation of a Au NP layer with lower density. Figure 3g shows the Raman results of 10^{-6} M R6G in the coffee ring from the above water-washed Au NP colloids. Clearly, the water-washed Au NP colloids with higher concentration times resulted in the worse performance of the coffee ring on SERS enhancement, which was

possibly due to the increased layer width, which would "dilute" the target molecules on the ring and thus decrease its SERS intensity. The ordinate in Figure 3g is the true Raman intensity of 10^{-6} M R6G in the coffee rings at the peak of 1364 cm^{-1}. It should be noted that the Raman intensity of R6G in Figures 3g and 4b do not correspond to each other since the data were collected from two Raman instruments (see details in the Materials and Methods). Since we mainly focused on the variation tendency of the SERS performance (Raman intensity) of the coffee ring for different concentration times of the washed Au NP colloids, the results from different instruments would not make a difference.

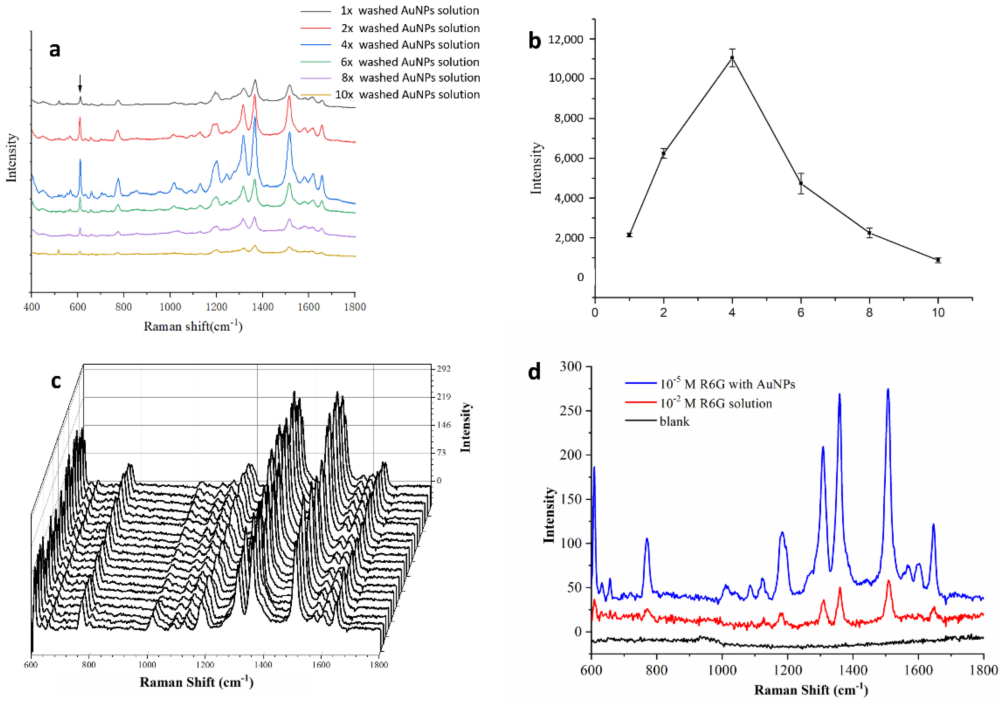

Figure 4. (**a**) Raman spectra of 10^{-5} M R6G in the coffee ring with 1×, 2×, 4×, 6×, 8× and 10× concentration water-washed Au NP colloids. (**b**)The tendency of Raman intensity of 10^{-5} M R6G in the coffee ring with water-washed Au NP colloids with different concentration times based on the peak of 1364 cm^{-1}. Data in a and b were collected from the Laser Raman spectrometer (Renishaw, UK): excitation wavelength, 785 nm; maximum excitation power, 5 mw; integration time, 10 s. (**c**) SERS intensity of 10^{-5} M R6G in the coffee ring measured in air, using laser excitation at 780 nm and 80 mW. (**d**) SERS intensity of 10^{-5} M R6G in the coffee ring, 10^{-2} M R6G solution and blank. Data in c and d were collected from the DXR Smart Raman spectrometer (Thermo Fisher Scientific, Waltham, MS, USA): excitation wavelength, 780 nm; maximum excitation power, 80 mw; integration time, 15 s.

To determine a more appropriate concentration of the water-washed Au NPs and obtain a better coffee ring effect, we tested the water-washed Au NP colloids at 1~10× concentration times very carefully. From the Raman results shown in Figure 4, it could be easily seen that for 4× concentration times of the water-washed Au NPs, the coffee ring presented the best performance. The Raman signals of 10^{-5} M R6G at the peak of 1364 cm^{-1} on such a coffee ring reached the strongest intensity under this condition, as shown in Figure 4b. These results suggest that relative to the as-prepared concentration, 4× concentration times of Au NP colloids enables one to fabricate a coffee ring with better Raman enhancement.

In addition to the concentration, the volume of droplets on the hydrophobic silicon wafer also has a certain impact on the number/distribution of hot spots formed at the edge of the coffee ring. For the same concentration of Au NP colloids, forming a complete ring will be difficult if the droplet volume is too small. A too-small droplet can also cause uneven hot spot distribution, which will no doubt affect the uniformity of SERS signals. However, dropping

too much will not increase the edge width of the ring, as presented in Figure S2c1–e1, but may induce multi-layer formation of the gold nanoparticles, which will degrade the performance of the coffee ring, as indicated in Figure 3. Figure S2f shows the Raman spectra of 10^{-5} M R6G within the ring for different droplet volumes of water-washed Au NP colloids with 4× concentration times. The coffee ring formed from a 1 µL droplet Au NP solution presents the highest performance based on the obtained peak intensity of R6G. Since it was difficult to take a droplet less than 1 µL in the practical operation, a water-washed Au NP colloid with 4 times concentration and a 1 µL droplet were selected as the optimum conditions to fabricate a coffee ring in the following experiments with the best performance on SERS enhancement. The signal uniformity and reproducibility of the optimized coffee-ring-based substrates were also evaluated with 10^{-5} M R6G at the 780 nm excitation wavelengths. The SERS response of R6G were relatively uniform, as shown in Figures 4c and S3. The relative standard deviations (RSDs) for peaks at 774 and 1305 cm^{-1}, for instance, were 14.6% and 17.1%, respectively.

The enhancement factor (EF) of the as-prepared coffee ring was calculated using the following equation: $EF = (I_{SERS}/I_{RS})\ (C_{RS}/C_{SERS})\ (MN_{RS}/MN_{SERS})$, where I_{SERS} is the SERS intensities of the intense band for R6G, I_{RS} is the normal Raman signal for the corresponding band of the R6G solution and C_{RS}/C_{SERS} is the concentration ratio of R6G in neat solution and on the coffee ring. MN_{RS}/MN_{SERS} is the molecular number of R6G in neat solution and on the coffee ring. Then, for this case, the EF of R6G for the as-prepared coffee ring is $EF = (260/41) \times (10^{-2}/10^{-5}) \times 2 = 1.2 \times 10^4$. The SERS intensity of 10^{-5}M R6G in the coffee ring, 10^{-2} M R6G solution and the blank are presented in Figure 4d. Since there are many factors which can influence the enhancement of the coffee rings, such as surface roughness, metal type (Au or Ag), nanoparticle sizes, surface modifications of nanoparticles, and so on [13,33], one can fabricate a better "coffee ring" by combining this method with other adjustment strategies for a special system.

To investigate the sensing performance of the as-prepared coffee ring under the optimized conditions, SERS spectra of a typical Raman reporter, R6G, with various concentrations were collected. As shown in Figure 5a, with an increasing concentration of R6G, distinct changes in the intensity were observed, including the intensity of the bands at 612 cm^{-1} (δ(CCC)), 774 cm^{-1} (δ(CH)) and 1509 cm^{-1} (ν(CC)). When taking the peak at 1509 cm^{-1} as a reference, the change in the intensity was found to be quantitatively correlated with the concentration of R6G, as shown in Figure 5b. Taking the limit of detection (LOD) as three times the standard deviation of the blank, the detection limit of the fabricated coffee ring for R6G could reach 5×10^{-8} M, indicating the sensitivity of this system.

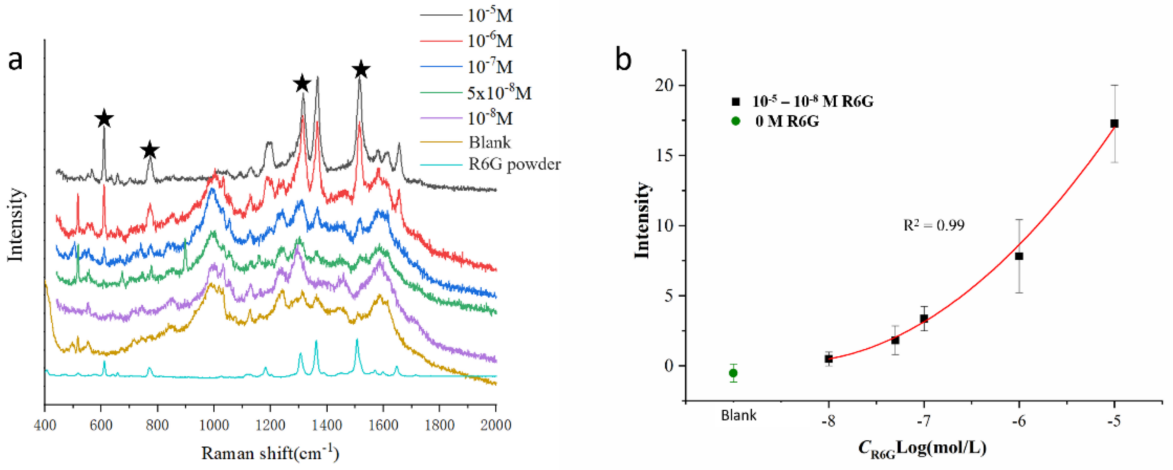

Figure 5. (**a**) Raman spectra of R6G with different concentrations in the optimized coffee ring substrate. The stars indicate the main fingerprint peaks of R6G in the coffee ring. (**b**) Semilog plot of the peak intensity as a function of R6G concentration for the peak of 1509 cm^{-1}.

An important test for this sensor is its performance in the sensing of target that is hard to detect. To assess this, we assayed AFB1 by using our fabricated coffee ring as the substrate. After spiking AFB1 with different concentrations to the water-washed Au NP colloids and preparing for the ring, Raman spectra were collected, and distinguishable Raman intensity changes were observed, especially at the peak of 1275 cm^{-1}, which corresponds to the bending and stretching vibration of C-H on the epoxy structure of aflatoxin. The peaks at 1551 cm^{-1} and 1592 cm^{-1}, corresponding to the C–C and C-C-C stretching mode and ring deformation [34], were also observable at the concentration of 10^{-6} M, as shown in Figure 6a. Noticeably, the intensity change in the peak at 1275 cm^{-1} was observed to quantitatively correlate with the AFB1 concentrations, as indicated in Figure 6b. The lin–log plot of intensity versus AFB1 concentration was linear over the range of 10^{-8} M—10^{-4} M AFB1. The results shown in Figure 6b clearly confirmed that our strategy could function well in AFB1 sensing with an LOD of 5×10^{-7} M.

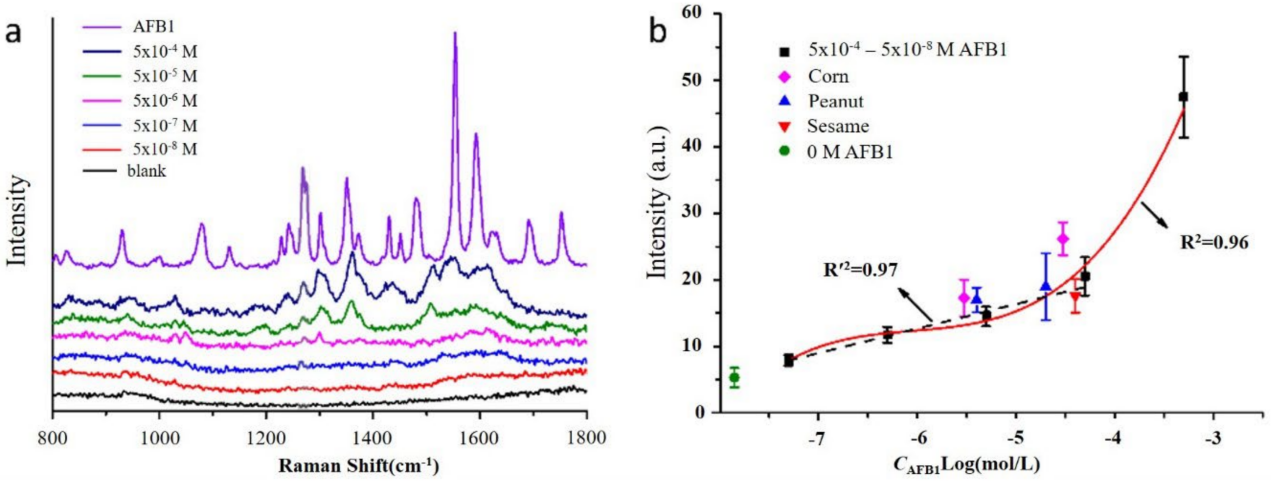

Figure 6. (**a**) Raman spectra of AFB1 with different concentrations in the optimized coffee ring substrate. (**b**) Semi-log plot of the peak intensity as a function of AFB1 concentration for the peak of 1275 cm^{-1}. The data were collected from the DXR Smart Raman spectrometer: (Thermo Fisher Scientific, Waltham, MS, USA) excitation wavelength, 780 nm; maximum excitation power, 80 mw; integration time 15 s.

More important in terms of potential applications of a sensor is testing the sensing capability in real-world situations. To assess this, we assayed an AFB1 concentration in peanut, corn flour and sesame, which are considered as the key objects for AFB1 pollution. The samples were firstly crushed into fine powders, then dispersed in water through vigorous stirring before centrifugation. When AFB1 with certain concentrations (see details in Experimental Section) was spiked into the real samples, the coffee ring was prepared and Raman spectra were collected. Distinct signals were observed, as indicated in Figure 6b. The detected Raman intensity for both peanut and sesame samples (the blue and red dots) spiked with certain AFB1 were very close to the semi-log plot, indicating the sensitivity of this platform. It should be noted that for corn samples, the collected Raman intensity was slightly higher than the semi-log plot, suggesting a little more AFB1 was involved in the corn samples. This could have been caused by the different sample preparation methods. That is, for peanut and sesame samples spiked with AFB1, the liquid supernatant was retained after solution centrifugation. Meanwhile, in the case of corn, the supernatant was taken in the absence of centrifugation. This meant the detected corn sample included some fine corn nanoparticles on which certain AFB1 molecules adsorbed and thus increased the detectable amount of AFB1, as indicated in Figure 6b. It was determined that the recovery of AFB1 for the real samples was in the range of 95–119%. The desirable results demonstrated the feasibility of the optimized coffee ring for the detection of AFB1 in practical applications. The standard deviations of the detected Raman intensity were relatively high for these

real samples as well as for the sample at a high concentration (C_{AFB1} = 10^{-3} M) on the working plot. This could have been due to the slight solubility and poor dispersion of AFB1 in aqueous solution. So, future work can focus on selecting a more appropriate medium/solvent that is transparent to Raman but can largely improve the solubility and dispersion of AFB1 in solution.

4. Conclusions

This work details the optimization of fabricating coffee rings to improve the sensitivity of coffee rings in detecting trace analytes on the basis of SERS technology. The results showed that the presence of sodium citrate in the gold colloid would have certain effect on the performance of the coffee ring. Furthermore, the concentration of gold particles (determined to be 4× concentration times as to the as-synthesized concentration) and the droplet volume (determined to be 1 µL) was explored to optimize the conditions for coffee ring fabrication. To the best of our knowledge, this is the first report on optimizing coffee ring formation. Using the coffee ring with the best properties as a SERS substrate, trace R6G with a concentration of 5 × 10^{-8} M was detected. This sensing platform can realize aflatoxin B1 (AFB1) detection to a concentration as low as 5 × 10^{-7} M. The high sensitivity of this platform was also presented in real-sample detection such as corn, peanut and sesame. We expect this sensor can not only be utilized for rapid detection in practical food products, but it will also have great potential to extend to label-free assays for other significant small molecules.

Supplementary Materials: The following supporting information can be downloaded at: https://www.mdpi.com/article/10.3390/chemosensors11010022/s1, Figure S1: Raman spectra of 10^{-6} M R6G with the coffee ring from 1×, 10×, 20×, 40×, 60× and 80× concentration water-washed AuNPs colloid; Figure S2: (a–e1) SEM images of the coffee ring formed from 4 times concentration water-washed AuNPs colloid with different droplet volumes. (f) Raman spectra of 10^{-5} M R6G in the ring in the case of different amount of the AuNPs droplet; Figure S3: SERS intensity for the corresponding bands of 3 substrates were assessed. Error bars indicate standard deviation of intensity from 20 randomly selected positions on 3 substrates.

Author Contributions: M.L. conceived the AFB1 detection strategy based on the coffee ring effect. X.Y. and W.Z implemented the optimization experiments of coffee ring fabrication and the R6G and AFB1 assay experiments and participated in data analysis. Y.W. (Yiran Wang) performed some measurements on AFB1 and participated in data analysis. D.K., participated in drawing the TOC and in valuable discussions on the optimization of coffee ring fabrication. X.Y., Y.W. (Yibing Wang) and M.L. wrote the manuscript and participated in valuable discussions. M.L. supervised the project. X.Y., W.Z. and Y.W. (Yibing Wang) have equally contributed to the work. All authors have read and agreed to the published version of the manuscript.

Funding: This work was supported by the National Basic Research Program of China (No. 2019YFB13 09703) and the National Natural Science Foundation of China (Grant Nos. 22074147, 22274157).

Data Availability Statement: Not applicable.

Conflicts of Interest: The authors declare that they have no known competing financial interests or personal relationships that could have appeared to influence the work reported in this paper.

References

1. Langer, J.; Jimenez de Aberasturi, D.; Aizpurua, J.; Alvarez-Puebla, R.A.; Auguié, B.; Baumberg, J.J.; Bazan, G.C.; Bell, S.E.J.; Boisen, A.; Brolo, A.G.; et al. Present and Future of Surface-Enhanced Raman Scattering. *ACS Nano* **2020**, *14*, 28–117. [CrossRef] [PubMed]
2. Xin, H.; Namgung, B.; Lee, L.P. Nanoplasmonic optical antennas for life sciences and medicine. *Nat. Rev. Mater.* **2018**, *3*, 228–243. [CrossRef]
3. Wang, X.; Huang, S.C.; Hu, S.; Yan, S.; Ren, B. Fundamental understanding and applications of plasmon-enhanced Raman spectroscopy. *Nat. Rev. Phys.* **2020**, *2*, 253–271. [CrossRef]
4. Sharma, B.; Frontiera, R.R.; Henry, A.I.; Ringe, E.; Duyne, R.P. SERS: Materials, applications, and the future. *Mater. Today.* **2012**, *15*, 16–25. [CrossRef]

5. Yamamoto, Y.S.; Ozaki, Y.; Itoh, T. Recent progress and frontiers in the electromagnetic mechanism of surface-enhanced Raman scattering. *J. Photochem. Photobiol. C Photochem. Rev.* **2014**, *21*, 81–104. [CrossRef]
6. Ding, S.Y.; Yi, J.; Li, J.F.; Ren, B.; Wu, D.Y.; Panneerselvam, R.; Tian, Z.Q. Nanostructure-based plasmon-enhanced Raman spectroscopy for surface analysis of materials. *Nat. Rev. Mater.* **2016**, *1*, 1–16. [CrossRef]
7. Granger, J.H.; Schlotter, N.E.; Crawford, A.C.; Porter, M.D. Prospects for point-of-care pathogen diagnostics using surface-enhanced Raman scattering (SERS). *Chem. Soc. Rev.* **2016**, *45*, 3865–3882. [CrossRef]
8. Kong, D.; Zhu, W.; Li, M. A facile and sensitive SERS-based platform for sulfite residues/SO2 detection in food. *Microchem. J.* **2021**, *165*, 106174. [CrossRef]
9. Nie, S.; Emory, S.R. Probing single molecules and single nanoparticles by surface-enhanced Raman scattering. *Science* **1997**, *275*, 1102–1106. [CrossRef]
10. Kneipp, K.; Wang, Y.; Kneipp, H.; Perelman, L.T.; Itzkan, I.; Dasari, R.R.; Feld, M.S. Single molecule detection using surface-enhanced Raman scattering (SERS). *Phys. Rev. Lett.* **1997**, *78*, 1667. [CrossRef]
11. Deegan, R.D.; Bakajin, O.; Dupont, T.F.; Huber, G.; Nagel, S.R.; Witten, T.A. Capillary flow as the cause of ring stains from dried liquid drops. *Nature* **1997**, *389*, 827. [CrossRef]
12. Choi, S.; Stassi, S.; Pisano, A.P.; Zohdi, T.I. Coffee-ring effect-based three dimensional patterning of micro/nanoparticle assembly with a single droplet. *Langmuir* **2010**, *26*, 11690–11698. [CrossRef]
13. Xu, J.; Du, J.; Jing, C.; Zhang, Y.; Cui, J. Facile detection of polycyclic aromatic hydrocarbons by a surface-enhanced Raman scattering sensor based on the Au coffee ring effect. *ACS Appl. Mater. Interfaces* **2014**, *6*, 6891–6897. [CrossRef]
14. Wang, W.; Yin, Y.; Tan, Z.; Liu, J. Coffee-ring effect-based simultaneous SERS substrate fabrication and analyte enrichment for trace analysis. *Nanoscale* **2014**, *6*, 9588–9593. [CrossRef]
15. Wu, J.; Zhang, L.; Bu, X.; Li, P.; Zhao, B.; Tian, Y. Determination of the illegal adulteration of natural healthcare products with chemical drugs using surface-enhanced Raman scattering. *Analyst* **2018**, *143*, 5202–5209. [CrossRef]
16. Gao, S.; Lin, Y.; Zhao, X.; Gao, J.; Xie, S.; Gong, W.; Yu, Y.; Lin, J. Label-free surface enhanced Raman spectroscopy analysis of blood serum via coffee ring effect for accurate diagnosis of cancers. *Acta Part A Mol. Biomol. Spectrosc.* **2022**, *267*, 120605. [CrossRef]
17. Pan, X.; Dong, J.; Li, Y.; Sun, X.; Yuan, C.; Qian, W. The strategy of two-scale interface enrichment for constructing ultrasensitive SERS substrates based on the coffee ring effect of AgNP@ β-CD. *RSC Adv.* **2016**, *6*, 29586–29591. [CrossRef]
18. Mata, A.T.; Ferreira, J.P.; Oliveira, B.R.; Batoréu, M.C.; Crespo, M.B.; Pereira, V.J.; Bronze, M.R. Bottled water: Analysis of mycotoxins by LC–MS/MS. *Food Chem.* **2015**, *176*, 455–464. [CrossRef]
19. Zhu, R.; Feussner, K.; Wu, T.; Yan, F.; Karlovsky, P.; Zheng, X. Detoxification of mycotoxin patulin by the yeast Rhodosporidium paludigenum. *Food Chem.* **2015**, *179*, 1–5. [CrossRef]
20. Zhang, X.; Li, C.R.; Wang, W.C.; Xue, J.; Huang, Y.L.; Yang, X.X.; Tan, Y.B.; Zhou, X.P.; Shao, C.; Ding, S.J.; et al. A novel electrochemical immunosensor for highly sensitive detection of aflatoxin B1 in corn using single-walled carbon nanotubes/chitosan. *Food Chem.* **2016**, *192*, 197–202. [CrossRef]
21. Ostry, V.; Malir, F.; Toman, J.; Grosse, Y. Mycotoxins as human carcinogens—The IARC Monographs classification. *Mycotoxin Res.* **2017**, *33*, 65–73. [CrossRef] [PubMed]
22. Vidal, J.C.; Bonel, L.; Ezquerra, A.; Hernández, S.; Bertolín, J.R.; Cubel, C.; Castillo, J.R. Electrochemical affinity biosensors for detection of mycotoxins: A review. *Biosens. Bioelectron.* **2013**, *49*, 146–158. [CrossRef] [PubMed]
23. Visconti, A.; Lattanzio, M.T.V.; Pascale, M.; Haidukowski, M. Analysis of T-2 and HT-2 toxins in cereal grains by immunoaffinity clean-up and liquid chromatography with fluorescence detection. *J. Chromatogr. A* **2005**, *1075*, 151–158. [CrossRef] [PubMed]
24. Anfossi, L.; Giovannoli, C.; Baggiani, C. Mycotoxin detection. *Curr. Opin. Biotechnol.* **2016**, *37*, 120–126. [CrossRef] [PubMed]
25. Zheng, Z.; Humphrey, W.C.; King, S.R.; Richard, J.L. Validation of an ELISA test kit for the detection of total aflatoxins in grain and grain products by comparison with HPLC. *Mycopathologia* **2005**, *159*, 255–263. [CrossRef]
26. Xie, L.; Chen, M.; Ying, Y. Development of methods for determination of aflatoxins. *Crit. Rev. Food Sci. Nutr.* **2016**, *56*, 2642–2664. [CrossRef]
27. Shkembi, X.; Svobodova, M.; Skouridou, V.; Bashammakh, A.S.; Alyoubi, A.O.; O'Sullivan, C.K. Aptasensors for mycotoxin detection: A review. *Anal. Biochem.* **2022**, *644*, 114156. [CrossRef]
28. Rossi, C.N.; Takabayashi, C.R.; Ono, M.A.; Saito, G.H.; Itano, E.N.; Kawamura, O.; Hirooka, E.Y.; Ono, E.Y.S. Immunoassay based on monoclonal antibody for aflatoxin detection in poultry feed. *Food Chem.* **2012**, *132*, 2211–2216. [CrossRef]
29. Taghdisi, S.M.; Danesh, N.M.; Ramezani, M.; Abnous, K. A new amplified fluorescent aptasensor based on hairpin structure of G-quadruplex oligonucleotide-Aptamer chimera and silica nanoparticles for sensitive detection of aflatoxin B1 in the grape juice. *Food Chem.* **2018**, *268*, 342–346. [CrossRef]
30. Bastús, N.G.; Comenge, J.; Puntes, V. Kinetically controlled seeded growth synthesis of citrate-stabilized gold nanoparticles of up to 200 nm: Size focusing versus Ostwald ripening. *Langmuir* **2011**, *27*, 11098–11105. [CrossRef]
31. Liu, Y.; Zhou, F.; Wang, H.; Huang, X.; Ling, D. Micro-coffee-ring-patterned fiber SERS probes and their in situ detection application in complex liquid environments. *Sensors Actuators B Chem.* **2019**, *299*, 126990. [CrossRef]
32. Yang, M.; Zou, Q.; Chen, D.; Hu, J.; Lin, Q.; Zhu, H. Factors of Importance for Arsenic Migration/Separation under Coffee-Ring Effect on Silver Nanofilms. *Langmuir* **2020**, *36*, 1662–1670. [CrossRef]

33. Murugesan, B.; Yang, J. Tunable Coffee Ring Formation on Polycarbonate Nanofiber Film for Sensitive SERS Detection of Phenylalanine in Urine. *ACS Omega* **2019**, *4*, 14928–14936. [CrossRef]
34. Wu, X.; Gao, S.; Wang, J.S.; Wang, H.; Huang, Y.W.; Zhao, Y. The surface-enhanced Raman spectra of aflatoxins: Spectral analysis, density functional theory calculation, detection and differentiation. *Analyst* **2012**, *137*, 4226–4234. [CrossRef]